Journal of Applied Fluid Mechanics, Vol. 18, No. 5, pp. 1231-1245, 2025.
Available online at www.jafmonline.net, ISSN 1735-3572, EISSN 1735-3645.
https://doi.org/10.47176/jafm.18.5.3074

Shape Optimization of Isosceles Triangle Facades for Improving the Aerodynamics of a Tall Building

M. Tabatabaei Malazi[1†] and K. Fakih[2]

[1]*Department of Mechanical Engineering, Faculty of Engineering, Istanbul Aydin University, Istanbul 34295, Turkey*
[2]*Energy Technologies Program, Institute of Graduate Studies, Istanbul Aydin University, Istanbul 34295, Turkey*

†*Corresponding Author Email: mahditabatabaei@aydin.edu.tr*

ABSTRACT

This study aims to investigate the simulation of wind impacts on a standard model of a tall building with a novel facades design. The tall building is established by the Commonwealth Advisory Aeronautical Council (CAARC). A substantial volume of data has been generated to improve the living conditions in a building measuring 182.9 m (H) x 45.7 m (B) x 30.5 m (D). A comprehensive investigation is conducted, including a total of 65 cases. These cases involve varying wind velocities, facade angles, and distances between the facades and the building. To verify the accuracy of the current results, the drag coefficient (C_D) values were compared in this study to those from previous experimental and numerical analyses published in the literature. The drag force, velocity, and pressure distribution surrounding the building were computed using computational fluid dynamics (CFD) techniques, considering various wind velocities and geometric characteristics. Research results reveal that both wind velocity and the geometric dimensions of the facades have an important influence on the drag force. The building experiences a significant increase in force as the wind velocity increases from 1 to 5 m/s. The results also indicate that the increasing angle of facades has a noticeable effect on increasing the force produced on the building. This data aims to achieve wind control through the passive flow control method, prevent weathering of the building, decrease wind load, facilitate natural ventilation, save energy, and provide building designers with a wide range of numerical simulations.

Article History

Received August 16, 2024
Revised December 9, 2024
Accepted December 19, 2024
Available online March 4, 2025

Keywords:

CFD
Wind
Facades
Buildings
Drag force

1. INTRODUCTION

The impact of wind on tall buildings is a critical factor in their design and construction. Utilizing facades can improve the aerodynamic efficiency of tall buildings and enhance natural building ventilation, reducing energy consumption. Zhao et al. (2024) reviewed wide-ranging studies on naturally ventilated double-skin façades (NVDSF). They demonstrated the benefits of NVDSF in reducing energy usage in building structures. Bianchi et al. (2024) addressed the academics' findings regarding facade design and optimization techniques. They discussed the use of conflicting criteria in facade design and the use of machine learning methods for facade optimization. Hou and Sarkar (2018) devised a time-domain methodology for predicting the forces and responses of tall buildings by utilizing aerodynamic parameters obtained from sectional model experiments. They tested the model in a wind tunnel to determine the parameters influencing the response of the CAARC Building. Pomaranzi et al. (2020) conducted a wind tunnel study to examine the aerodynamic performance of a corrugated double-skinned building facade. They discovered that the amplitude of pressure fluctuations is dependent on both U_∞ and the geometry of the groove. Reducing cyclic pressure fluctuations caused by vorticity formation in cavities reduced peak values by 40%. Jafari and Alipour (2021) generated an initial dataset to create smart morphing facades (known as Smorphacades) for tall structures with rectangular and elliptical forms. They used experimental methodology to generate a dataset from CFD simulations, created a prediction model, and determined the ideal Smorphacade shape, demonstrating its effectiveness in reducing wind-induced drag forces. Amani-Beni et al. (2024) carried out a comprehensive study to simulate wind effects on a tall building model with facades. The research looks to improve living circumstances by implementing passive flow management, which decreases building

NOMENCLATURE

A	distance between the front face of the building and facades	M	distance between Facades
B	building Length	U∞	wind velocity
C	length of facade	2D	two-dimensional
CAARC	Commonwealth Advisory Aeronautical Council	3D	three-dimensional
CFD	Computational Fluid Dynamics	α	angle of isosceles triangle facades
C_D	drag coefficient	β	angle of wind-inlet

deterioration, minimizes wind loads, and enhances energy savings and ventilation by nature. The research results revealed that passive flow control significantly reduces wind-induced drag forces. Fuliotto et al. (2010) carried out numerical analyses of the flow that interacted with a building facade consisting of multiple levels, both in two-dimensional and three-dimensional. They revealed that the two-dimensional numerical analysis provided highly accurate results due to the flow's nearly two-dimensional nature. Pasut and Carli (2012) conducted a study and concluded that there was no statistically significant distinction in the temperature and velocity patterns in the analyzed flow fields when comparing two-dimensional and three-dimensional numerical calculations. Lops et al. (2021) reached the same conclusion in their numerical investigations. Accepting the flow as two-dimensional reduces the computing load on the computer, enabling the execution of additional processes. The study suggests that increasing the number of parameters to be evaluated within a specific timeframe can enhance the creation of a more significant curve. Using wind tunnel experiments, Yuan et al. (2018) investigated the impact of façade appurtenances on local peak wind pressures in high-rise buildings. They simulated 21 appurtenance configurations using thin horizontal splitter plates. The results demonstrated that changes in plate vertical distance can significantly influence the locations of the largest positive peak pressures. Appurtenances reduced the largest negative peak pressure by 42% on the higher leading corner and the entire side face. Hou et al. (2023) described a smart-morphing-façade (Smorphacade) method to reduce wind-induced vibrations in tall structures. The system consists of circular ducts arranged in a matrix within a flat plate. The system's efficacy in mitigating building response ranged from 16.7% to 18.6%, with a maximum decrease of 32% and 59.7% in the across-wind and torsional directions, respectively. Factors such as Smorphacade configuration, wind speed, and angle of attack influenced these reductions. Attia et al. (2018) carried out a study on adapted facades, focusing on their performance evaluation. They identified deficiencies and introduced an innovative approach to characterize facades based on objects. The research examined stakeholders, process diagrams, and insights from industry professionals. The results highlighted the importance of effective design, operation, and maintenance for energy conservation and occupant satisfaction, emphasizing the need for future challenges. Škvorc and Kozmar (2023) investigated wind loads on tall buildings with porous double-skin façade systems. They carried out experiments in a boundary-layer wind tunnel and created two atmospheric boundary layer (ABL) simulations. They show that rural ABL simulations yield larger mean pressure coefficients, whereas suburban ABL simulations cause a higher standard deviation. In their study, Chen et al. (2022) examined high-rise buildings and discovered that alterations in façade appurtenances have a substantial impact on wind pressure, resulting in a maximum decrease of 21%. The average wind pressure impact is less noticeable. Vertical strips can reduce the level of horizontal coherence to a maximum of 38%. Nevertheless, the impact on vertical coherence is quite minor. Hosseini et al. (2019) introduced active occupant interaction in responsive façades, focusing on interactive functionalities. They used qualitative and quantitative methodologies to design kinetic façade structures for real-time daylight management. The kinetic interactive façade can be transformed by adjusting dynamic daylight and occupant position, ensuring optimal visual comfort. Simulation findings showed three-dimensional modifications significantly improved visual comfort. Yi and Kim (2021) utilized a reversible 4D-printed material to enable flexible climate adaptation in buildings. The study explores the creation and operation of a responsive façade using thermoresponsive shape-memory composites (SMCs), utilizing digital modeling and practical observation to evaluate the material's performance, highlighting the potential of smart materials and 4D printing. Soudian and Berardi (2021) developed a new approach to climate-responsive facades (CRFs) for high-performance building facade design, focusing on selecting suitable technologies for multifunctional CRFs. The framework includes five steps: defining objectives, setting performance constraints, defining a responsive operation scenario, selecting suitable technology, and creating a conceptual design. Chaudhry et al. (2015) utilized CFD to analyze the Bahrain Trade Centre's architectural domain, determining the capacity of building-integrated wind turbines to generate power. The study found that the benchmark model generated an estimated 6.4 kW of power, with a capacity factor of 2.9%. Turbulence intensity increased inversely proportional to building height, with turbines at higher altitudes experiencing the most wind exposure.

Mallick et al. (2018) simulated the impact of wind on C-shaped buildings and optimized it by adjusting the angle of incidence. The study used ANSYS Fluent software for numerical analysis, focusing on the k-ε turbulence model and CFD techniques, proving that CFD is an efficient and accurate method for predicting wind pressure in buildings.

This highlights a significant deficiency in the literature regarding numerical simulations of the effects of various facade shapes on buildings using the CFD method. The novelty of this paper points to how to use basic geometric

shapes, specifically isosceles triangles, to design facades at various angles and configurations. Sixty-five original numerical simulation examples were conducted to systematically figure out wind behavior around buildings with facades, following validation against the most recent literature. The CAARC specifies a standard tall building with dimensions of 182.9 m x 45.7 m x 30.5 m. This corresponds to the building model dimensions of 1.829 m x 0.457 m x 0.305 m, obtained by reducing the actual building size by 1/100. Note that Hou and Sarkar (2018) and Jafari and Alipour (2021) have also conducted experimental and numerical studies on the aerodynamics of similar structures. The main focus of this work is the design of the segmented covering materials (facades) in response to different wind loads. A detailed examination of the building's design and its facades has been carried out using CFD simulations to improve our knowledge of the flow characteristics surrounding the building and its facades. The building, with facades shaped like isosceles triangles with angles of 15°, 30°, and 45°, was chosen as a benchmark to consider different characteristics. The building with facades in the shape of isosceles triangles was solved using a realizable k-ε turbulence model. The simulations were conducted at five distinct wind velocities (U_∞ = 1 m/s, 2 m/s, 3 m/s, 4 m/s, and 5 m/s) and three different wind-inlet angles (0°, 45°, and 90°). This study presents valuable insights into the ways in which facades can improve building design by functioning as windbreaks, helping natural ventilation, optimizing energy efficiency, and influencing microclimates. The study's findings demonstrate that CFD models can solve wind flow issues around buildings and facades in a variety of geometries and in real building dimensions. Minimizing drag forces on buildings can facilitate the utilization of lighter materials. Consequently, the costs associated with building construction drop. In the present study, we consider the impact of wind-induced forces on a high-rise building model featuring facades, with the aim of determining the optimal dimensions of isosceles triangle facades to reduce drag forces.

The paper was structured in the following steps: Section 2 contains a definition for governing equations, computational regions, and computational techniques. Section 3 presents the numerical model's verification, computation results, and subsequent discussions. Section 4 includes the study's conclusions.

2. MATERIALS AND METHODS

Equations of Governance

The CFD models can be used to simulate the surrounding airflow acting on buildings with facades. These models can efficiently resolve intricate aerodynamic problems rapidly, with minimal computing cost and optimal accuracy. The CFD models can predict outcomes like velocity and pressure distribution surrounding the building's structure once they apply acceptable boundary conditions, such as wind direction and velocity.

The realizable k-ε turbulence model was used to simulate turbulent flow in a two-dimensional computational fluid area (ANSYS Fluent Theory Guide, 2013; Olcay & Tabatabaei Malazi, 2016). The formulas for continuity and momentum can be written as:

$$\frac{\partial \rho}{\partial t} + \frac{\partial (\rho u_i)}{\partial x_i} = 0 \tag{1}$$

$$\frac{\partial (\rho u_i)}{\partial t} + \frac{\partial \left(\rho u_i u_j\right)}{\partial x_j} = -\frac{\partial P}{\partial x_i} + \rho g_i + \frac{\partial}{\partial x_j}(\mu + \mu_t) \left(\frac{\partial u_i}{\partial x_j} + \frac{\partial u_j}{\partial x_i}\right) + S_i \tag{2}$$

Where ρ shows the density. u_i *and* u_j illustrate the average velocity component of the fluid. P represents pressure, S_i represent the source term for the momentum equation, μ illustrates the dynamic viscosity, μ_t shows the eddy viscosity, and it is computed as $\mu_t = \rho C_\mu \frac{k^2}{\varepsilon}$. The transport equation for k and ε for the realizable k−ε model can be expressed as,

$$\frac{\partial}{\partial t}(\rho k) + \frac{\partial}{\partial x_i}(\rho k u_i) = \frac{\partial}{\partial x_j}\left[\left(\mu + \frac{\mu_t}{\sigma_k}\right)\frac{\partial k}{\partial x_j}\right] + G_k + G_b - \rho\varepsilon - Y_M + S_k \tag{3}$$

$$\frac{\partial}{\partial t}(\rho \varepsilon) + \frac{\partial}{\partial x_i}(\rho \varepsilon u_i) = \frac{\partial}{\partial x_j}\left[(\mu + \frac{\mu_t}{\sigma_\varepsilon})\frac{\partial \varepsilon}{\partial x_j}\right] + C_{1\varepsilon}\frac{\varepsilon}{k}(G_k + C_{3\varepsilon}G_b) - C_{2\varepsilon}\rho\frac{\varepsilon^2}{k} + S_\varepsilon \tag{4}$$

where k illustrates the turbulent kinetic energy. ε illustrates rate of dissipation. G_k shows turbulent kinetic energy generation, G_b shows turbulent kinetic energy generation, and Y_M repesents fluctuating dilatation contribution to the overall dissipation rate. The model parameters for realizable k-ε turbulence model can be defined $C_{1\varepsilon} = 1.44$, $C_{2\varepsilon} = 1.92$, $\sigma_k = 1.0$, $C_\mu = 0.09$, and $\sigma_\varepsilon = 1.3$.

Computational Techniques, Meshing, and Boundary Conditions

Figure 1 presents a three-dimensional schematic drawing of the building with isosceles triangle facades. Figure 2 illustrates the two-dimensional geometric templates used for computational simulations, including information about the boundary conditions. Figure 3 and Table 1 provide comprehensive measurements of the building's dimensions and exterior. Here, the building has dimensions of 0.457 meters in length and 0.305 meters in width. The choice of computational domain size is a

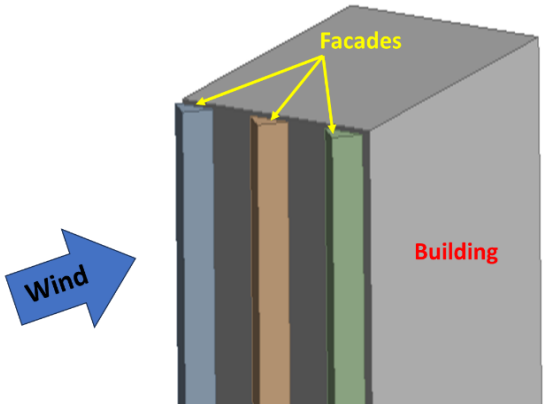

Fig. 1 A 3D view of a schematic drawing of a building combined with isosceles triangle facades

Table 1 Details of the model building dimensions considered in the present study

Symbol	Value	Detail
A	0.02, 0.01 (m)	Distance between the front face of the building and facades
B	0.457 (m)	Building Length
D	0.305 (m)	Building Width
M_1 , M_2	0.061 (m)	Distance between Facades
C	0.061 (m)	Length of facade
α	15º, 30º, 45º	Angle of an isosceles triangle facade

Table 2 Numerical simulations carried out in the present study

Model	A (m)	α	β	U_∞ (m/s)
Building without Facades		-	0º, 45º, 90º	1, 2, 3, 4, 5
Building with facades	0.02, 0.01	15º, 30º, 45º	0º	1, 2, 3, 4, 5
Building with facades	0.02, 0.01	45º	45º, 90º	1, 2, 3, 4, 5

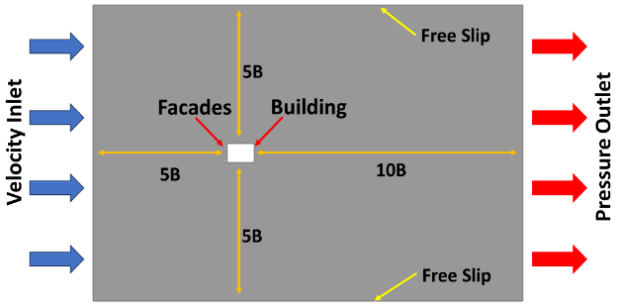

Fig. 2 A 2D view of the computational region and boundary conditions

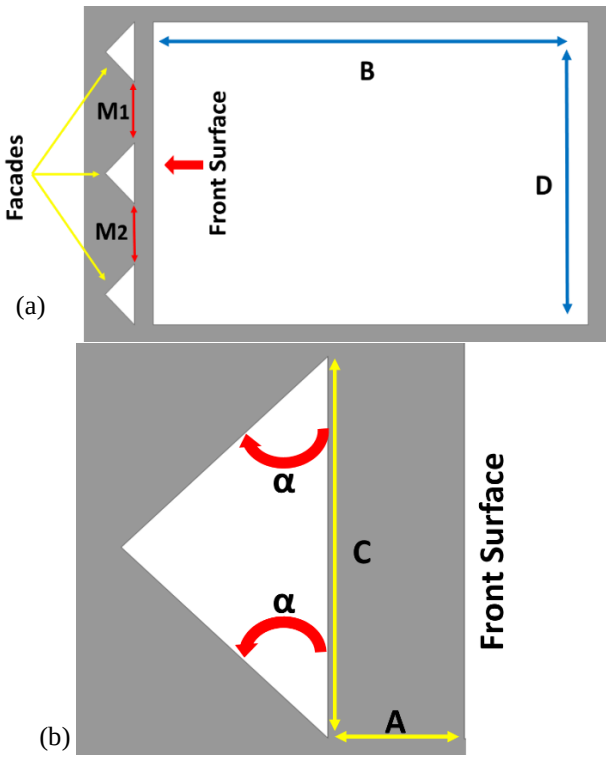

Fig. 3 (a) Specifics of the buildings with isosceles triangle facades, and (b) an enlarged view of an isosceles triangle façade

critical factor in wind analysis studies of buildings. In this study, a rectangular computational domain was chosen with a length and width of 16B and 9B, respectively. The building was situated 5B downstream from the velocity inlet cross-section and 10B upstream from the pressure outlet cross-section in the computational region. The side edges of the computational region were selected as a free-slip boundary condition. A no-slip boundary condition was utilized for the building and its facade walls. The facades were designed in the shape of isosceles triangles. Three varying angles were used for isosceles triangle facades (α = 15º, 30º, and 45º). The distance between the isosceles triangle facades and the building's front wall was determined to be between 0.01 and 0.02m. This study investigated various wind velocities (U_∞ = 1 m/s, 2 m/s, 3 m/s, 4 m/s, and 5 m/s) at three different wind-inlet angles (0°, 45°, and 90°) for inlet airflow. First, the building with and without facades were examined under five distinct wind velocities (U_∞ = 1 m/s, 2 m/s, 3 m/s, 4 m/s, and 5 m/s) and three different angles of the isosceles triangle facades (α = 15º, 30º, and 45º), with a wind-inlet angle of 0°. Then, the building with isosceles triangle facades at angles of 45° was chosen for modeling at various wind-inlet angles so the building with isosceles triangle facades at angles of 45° was simulated at five different wind velocities (U_∞ = 1 m/s, 2 m/s, 3 m/s, 4 m/s, and 5 m/s), as well as wind-inlet angles of 45° and 90°. The study investigated a total of 65 numerical simulation cases, out of which 15 were analyzed without isosceles triangle facades. Additionally, 50 numerical simulation cases were run at three various isosceles triangle facades (α), two distances between the isosceles triangle facades and the building's front wall (A), five different wind velocities (U_∞), and three different wind-inlet angles for inlet airflow (β).

A brief description of all the numerical simulations is provided in Table 2.

The Ansys Fluent commercial software was employed to solve the governing equations in the steady-state airflow domain. The fluid domain was calculated using the pressure-based solver type and the coupled scheme. The governing equations were considered to have converged when the minimum criterion of 10^6 as reached. The continuity and momentum equations were all competently solved until the convergence criteria were reached.

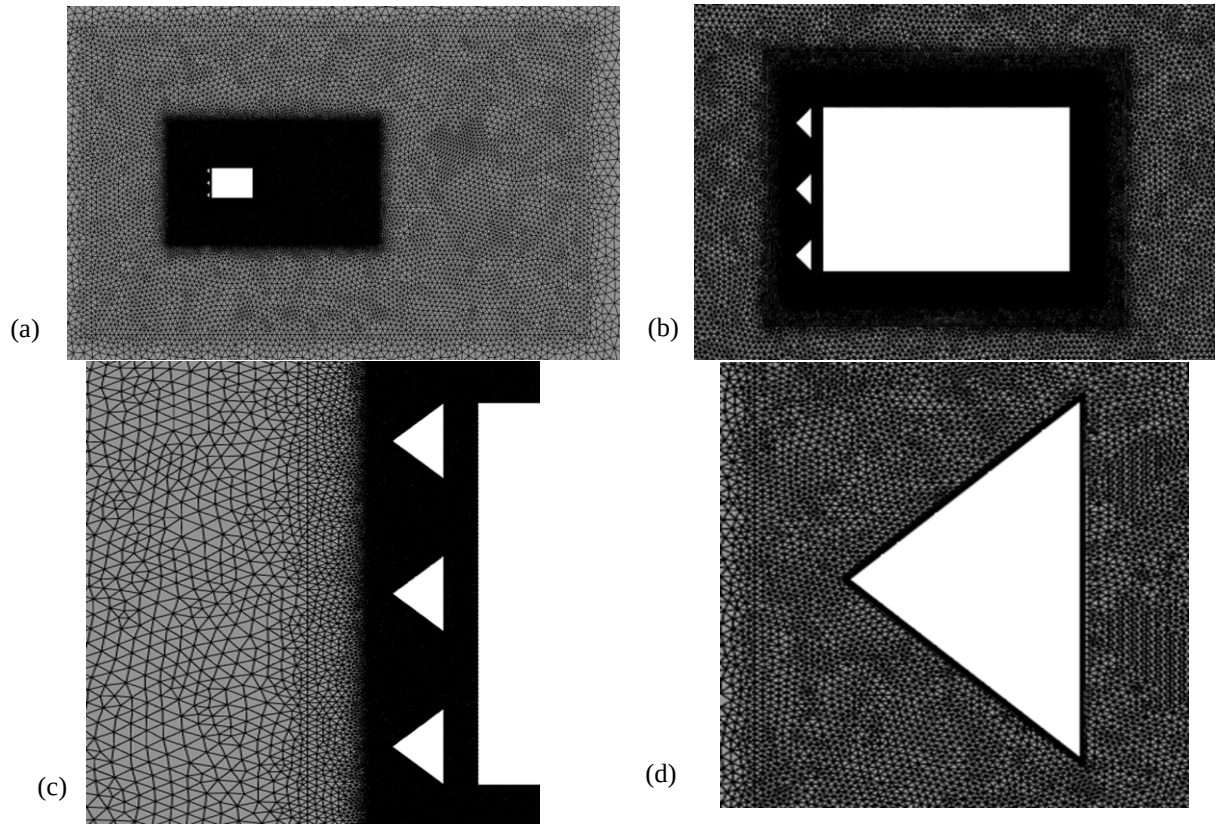

Fig. 4 (a) Cross-section of mesh domain, (b) enlarged view of the mesh around buildings, (c) enlarged view of the mesh near facades, (d) enlarged view of the mesh around facades

Figure 4 illustrates a mesh that contains both triangular and quadrilateral components, which has been generated for the computational fluid domain. The multi-block mesh construction method was utilized to divide the solution area into multiple parts. A high-density triangle mesh encircled the building and its isosceles triangle facades, while a quadrilateral mesh covered the walls. Mesh independence tests, specifically considering the drag force value at a wind velocity of 5 m/s, isosceles triangle facades at angles of 15°, and wind-inlet at an angle of 0°, confirmed the simulations' accuracy, as shown in Table 3. A total of 300.000 thousand elements were used in the solution area for 65 various models. These models achieved an error rate of under one percent at various U_∞ and α values.

Hou and Sarkar (2018) conducted experimental research on the aerodynamics of identical buildings, whereas Jafari and Alipour (2021) conducted numerical investigations. Both studies scaled down the original building's size by a reduction factor of 1/400. In this research, the CAARC defines a typical tall building with dimensions of 182.9 meters in length, 45.7 meters in width, and 30.5 meters in height. The building model dimensions of 0.457 m x 0.114 m x 0.076 m are identical to the real building size, which has decreased by a factor of 1/400. This reduction allows for accurate comparisons with the experimental and numerical results mentioned above. Nevertheless, Hou and Sarkar (2018), Jafari and Alipour (2021) and Amani-Beni et al (2024) fulfilled the drag coefficient in the two-dimensional model with a B value of 0.114 m and a D value of 0.076 m at a Reynolds number of 6.24×10^4. We compared the results of the drag coefficient values from the present research to those from previous experimental and numerical investigations by Hou and Sarkar (2018), Jafari and Alipour (2021) and Amani-Beni et al (2024) to confirm the validity and accuracy of the method. Table 4 reveals a comparison study of the drag coefficient result between the present study and previous studies when wind directions are 0 and 90 for Re of 6.24×10^4. The comparison demonstrates a good correlation between the present work and the experimental and numerical results presented by Hou and Sarkar (2018), Jafari and Alipour (2021) and Amani-Beni et al (2024).

Table 3. Details of mesh independence study

Mesh resolution	Drag force (N)	% Difference
220.000 elements	8.05	11
280.000 elements	7.68	4.8
300,000 elements	7.61	0.91

3. Results and Discussion

3.1 Aerodynamic Forces Study

When a wind impacts a building, it can generate a drag force on the building (Batchelor, 2000; Tabatabaei Malazi et al., 2020; Amani-Beni et al., 2023). The value of the FD can be calculated using the formula as follows:

Table 4 Comparison of previous experimental and numerical results of drag force with the present study

β	Experiment (Hou & Sarkar, 2018)	Numerical (Jafari & Alipour, 2021)	Numerical (Amani-Beni et al, 2024)	Present study	Error (%)
0	-	1.270	-	1.281	0.86
0	-	-	1.274	1.281	0.55
0	1.250	-	-	1.281	2.41
90	-	2.828	-	2.848	0.70
90		-	2.857	2.848	0.31
90	2.926	-	-	2.848	2.73

$$F_D = F_{D\_pressure} + F_{D\_viscous} = \oint P\,\hat{n}\,.\,\hat{e}_d dS + \oint \tau_w\,\hat{t}\,.\,\hat{e}_d dS \quad (7)$$

where $F_{D\_pressure}$ illustrates the pressure drag, $F_{D\_viscous}$ represents the viscous drag, p and τ illustrate the pressure and the wall shear stress.

Figures 5–8 exhibit the drag forces under various conditions, including varying wind velocity (U_∞=1 m/s, 2 m/s, 3 m/s, 4 m/s, and 5 m/s), isosceles triangle facades (15°, 30°, and 45°), and distances (A = 0.01 m and 0.02 m) between the front surface of the building and the isosceles triangle facades when the wind-inlet angle is 0°. It has been accepted that when the incident flow velocity (U_∞) is perpendicular to the frontal wall surface, the highest drag force on the frontal wall of the model building is caused by the stagnation pressure. The model building, both with and without isosceles triangle facades, converts the kinetic energy of the incoming airflow into pressure energy. The pressure applied to the wall's surface generates a force known as drag, which acts in the opposite direction from the wall. Typically, the architectural design of a building integrates facades, considering both thermal efficiency and visual appeal. For all variations of the building with isosceles triangle facades, the drag force increases with an increase in wind velocity. As wind velocity increases, drag forces on the isosceles triangle facades also rise (Figs 5a, 6a, and 7a). The drag forces at isosceles triangle facades at angles of 15° are greater than the drag forces at isosceles triangle facades at angles of 30° and 45°, when considering the drag forces acting on the isosceles triangle facades. The walls of an isosceles triangle facade with 45° angles experience lower pressure forces compared to those with 15° angles. An isosceles triangle facade, with 15° angles, behaves similarly to a plate against wind. On the other hand, when the angles of the isosceles triangle facade change from 15° degrees to 45° degrees, the pressure on the walls decreases. It is clear that an isosceles triangle facade with a 45° angle has a better aerodynamic shape than an isosceles triangle facade with a 15° or 30° angle because it can show less resistance to airflow. Figures 5b, 6b, and 7b illustrate that the building with isosceles triangle facades has lower drag forces than the building without isosceles triangle facades when the drag force is considered only on the building. In this situation, the frontal wall area experiences a minimal amount of drag force because isosceles triangle facades act like a shield and block the wind. Figures 5c, 6c, and 7c depict the total drag forces acting on the building with isosceles triangle facades. The total drag forces of the building with

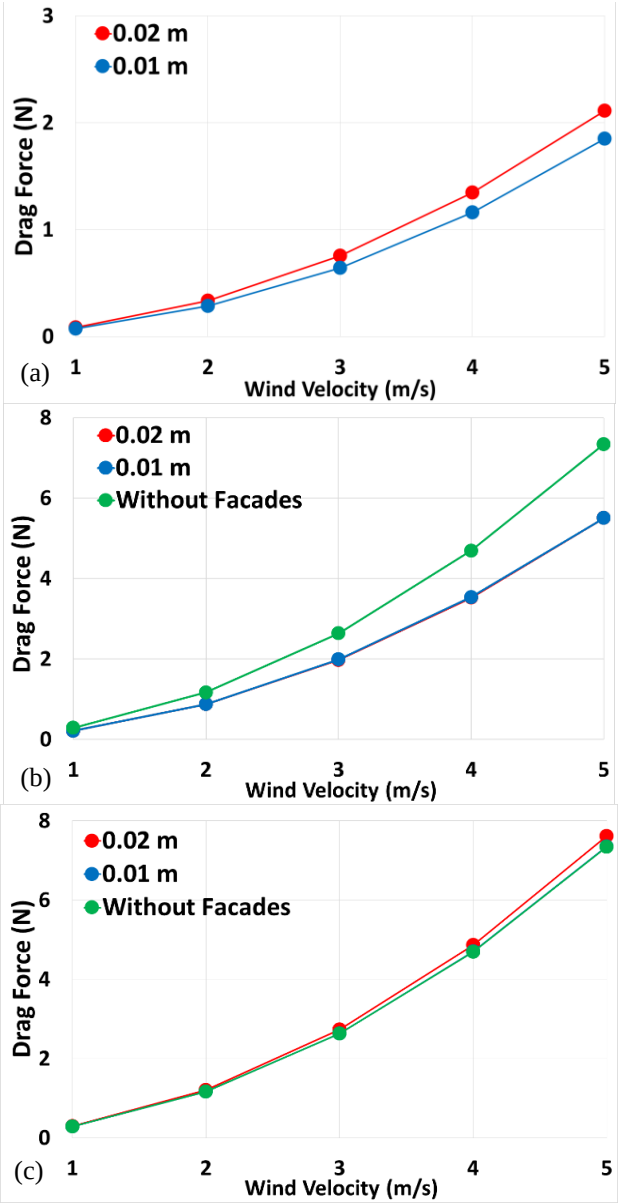

Fig. 5 Drag forces vary with different wind velocities at α = 15° and β = 0°, (a) isosceles triangle facades, (b) building, and (c) building with isosceles triangle facades

isosceles triangle facades at angles of 15° are greater than the drag forces of the building without isosceles triangle facades when the total drag forces are considered in the building and its isosceles triangle facades. On the other hand, the total drag forces of the building with isosceles triangle facades at angles of 30° and 45° are

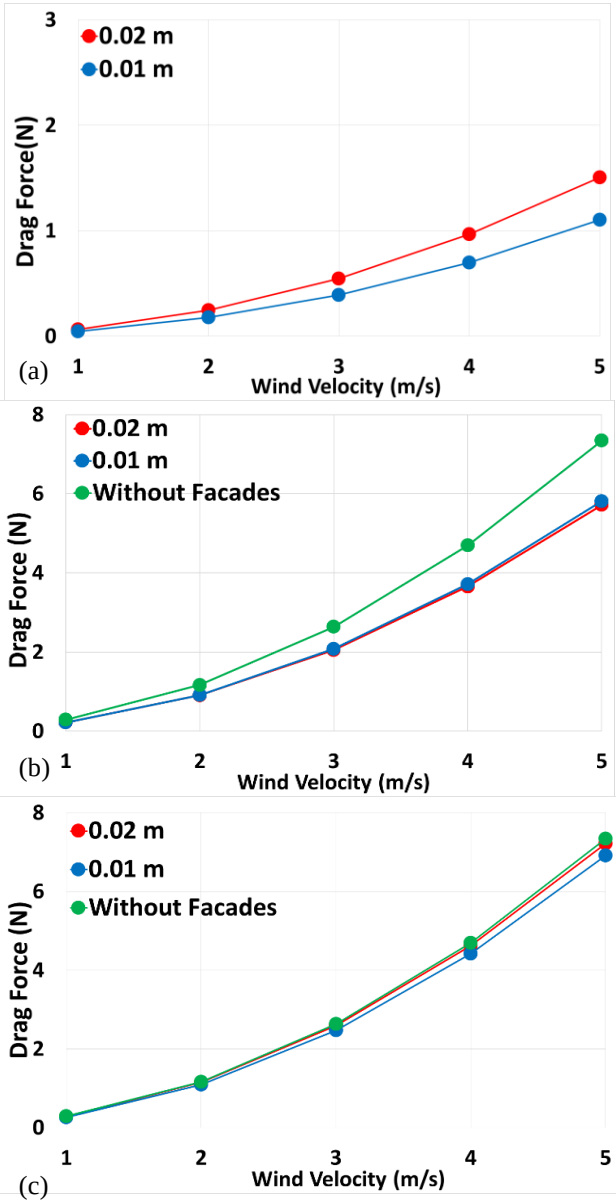

Fig. 6 Drag forces vary with different wind velocities at α = 30° and β = 0°, (a) isosceles triangle facades, (b) building, and (c) building with isosceles triangle facades

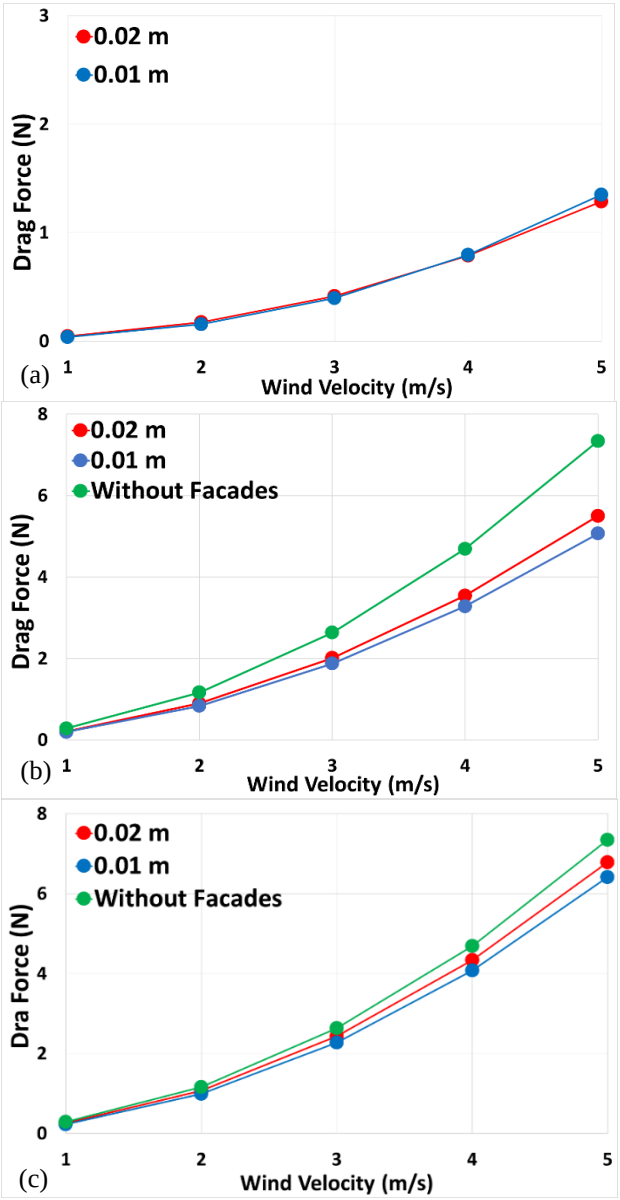

Fig 7 Drag forces vary with different wind velocities at α = 15° and β = 0°, (a) isosceles triangle facades, (b) building, and (c) building with isosceles triangle facades

smaller than the drag forces of the building without isosceles triangle facades when the total drag force is considered for the building and its isosceles triangle facades. It is understood that the difference in total drag forces between the building without isosceles triangle facades and the building with isosceles triangle facades becomes greater as the wind velocity increases. When the isosceles triangle facade angle is 45°, we observe the largest difference in total drag forces between the building without isosceles triangle facades and the building with isosceles triangle facades. As the distance between the building's front surface and the isosceles triangle facades increases, the drag force increases in all models. The building with isosceles triangle facades generates higher total drag forces when the distance between the front surface and the facades is 0.02 m, compared to when it is 0.01 m. The facades situated 0.2 m from the wall provide airflow through open gaps between the building's front wall and the facades, so the front face of the building can endure significant pressure forces. Figure 8 represents a comparison of the drag forces of the building with isosceles triangle facades at three distinct angles of 15°, 30°, and 45°. At all wind velocities, the building with isosceles triangle facades at angles of 15° experiences higher total drag forces than the building with isosceles triangle facades at angles of 30° and 45°.When the wind velocity is 5 m/s, the drag force of the building with isosceles triangle facades at angles of 15° is nearly 12% greater than the drag force of the building with isosceles triangle facades at angles of 45° when the distance between the front surface of the building and the isosceles triangle facades is 0.02 m. In addition, this rate becomes 14% when the distance between the front surface of the building and the isosceles triangle facades is 0.01 m. The

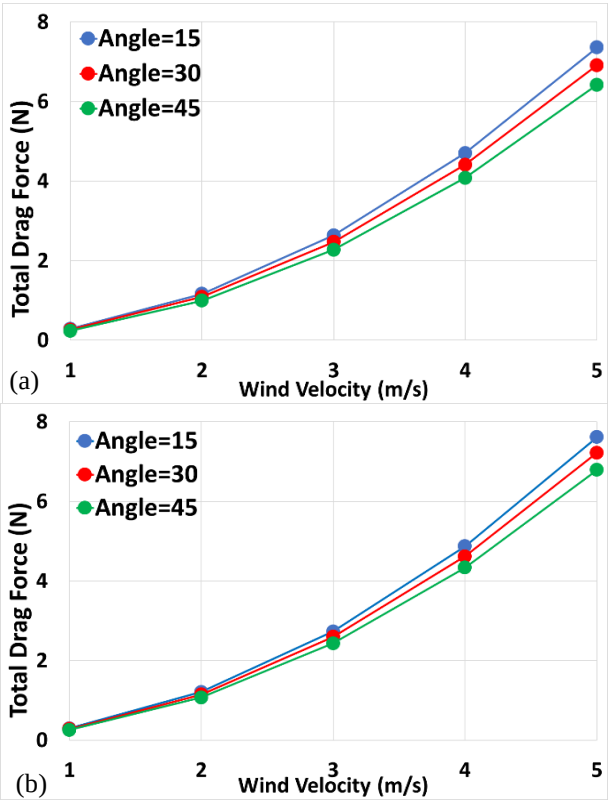

Fig. 8 Comparison drag forces vary with different wind velocities at α = 15°, 30°, and 45° with β = 0°, (a) 0.01 m distances, and (b) 0.02 m distances

drag force of the facade and building is significantly affected by the angles of the isosceles triangle facades. A review of the models shows that the drag forces results are significantly influenced by the angle of the isosceles triangle facades, rather than the distance between the building's front surface and the facades.

Wall surface dimensions determine the value of the pressure force that airflow creates. The magnitude of the pressure force increases with the growth of wall surface dimensions. The drag force on the building rises with the growth of the pressure force. Figures 9–11 illustrate the impact of the wind-inlet angle on drag forces. As the wind-inlet angle shifts from 0° to 90° degrees, the surface area opposing the wind becomes larger, resulting in a growth in drag forces. This section considers the inlet airflow with wind-inlet at angles of 45° and 90° for the building with isosceles triangle facades at angles of 45°. Figure 9a concludes that the isosceles triangle facades with a 45° wind-inlet angle exhibit less drag force than those with a 0° wind-inlet angle. Figure 9b demonstrates that the use of isosceles triangle facades on a building reduces drag forces compared to a building without isosceles triangle facades, specifically when considering drag force alone on the building. Figure 9c shows that the total drag forces created by the building with isosceles triangle facades are nearly equal for two different distances between the building's front surface and the isosceles triangle facades (A = 0.01 and 0.02 m). Figure 10 makes it clear that drag forces on the building's isosceles triangle facades are lower when the wind-inlet angle is 90° than when it is 0° or 45°. On the other hand, the drag forces acting on the

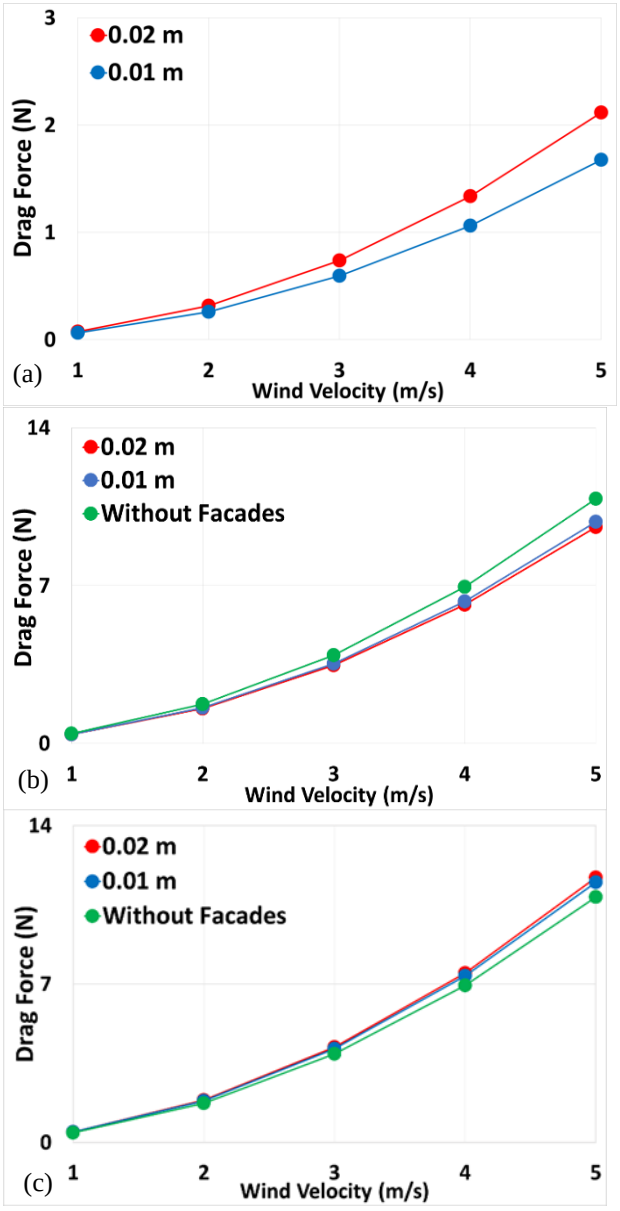

Fig. 9 Drag forces vary with different wind velocities at isosceles triangle facades with β = 45°, (a) isosceles triangle facades, (b) building, and (c) building with isosceles triangle facades

building are greater when the wind-inlet angle is 90° than when it is 0° or 45°. The building's contact surface with the airflow increases at a wind-inlet angle of 90° compared to a wind-inlet angle of 0°. Figure 11 displays a comparison of the drag forces acting on the building with isosceles triangle facades at angles of 45°, with the wind-inlet angle set at 0°, 45°, and 90°. The drag force acting on the building and its isosceles triangle facades at a wind velocity of 5 m/s is about 79% more at a wind-inlet angle of 45° than it is at 0°. This variation in drag force occur at a distance of 0.01 m between the facades and the front surface of the structure. Furthermore, at a distance of 0.02 m from the building's front surface to its facades, this percentage becomes to 73%. The angle at which the wind enters strongly influences the drag force. At a wind velocity of 5 m/s, the drag force on the building and its isosceles triangle facades is approximately 88% higher

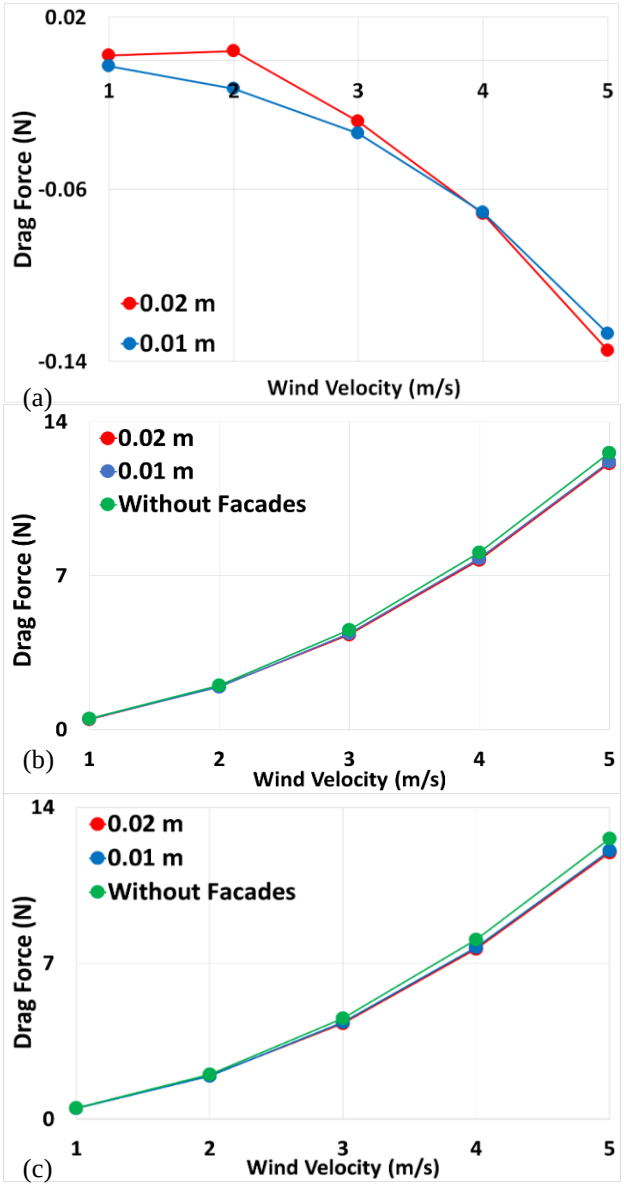

Fig. 10 Drag forces vary with different wind velocities at isosceles triangle facades with β = 90°, (a) isosceles triangle facades, (b) building, and (c) building with isosceles triangle facades

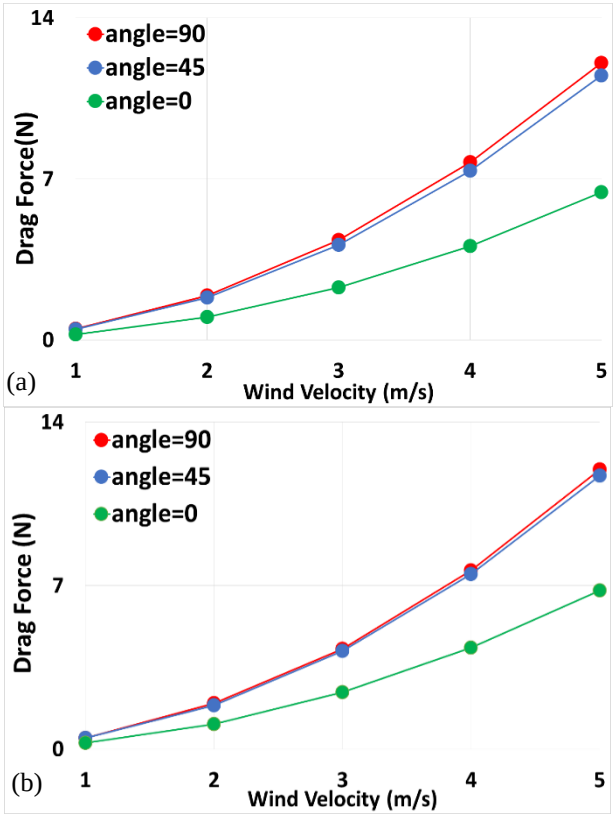

Fig. 11 Comparison drag forces vary with different wind velocities with β = 0°, 45°, and 90°, (a) 0.01 m distances, and (b) 0.02 m distances

when the wind-inlet angle is 90° compared to when it is 0°. This difference in drag force occurs when the distance between the building's front surface and the facades is 0.01 m. In addition, this rate changes to 76% when the distance between the front surface of the building and the facades is 0.02 m. The comparison of the models highlights that the wind-inlet angle, especially at 90°, dramatically impacts the drag force outcomes.

3.2 Velocity and Pressure Contour Plots of the Numerical Study

Figures 12–14 depict a comparison of the velocity contour plots around the building model. The comparison is made between the model without isosceles triangle facades and the model with isosceles triangle facades when the wind-inlet angle is set at 0° and the isosceles triangle facades are at three different angles: 15°, 30°, and 45°. The comparison was conducted at three distinct wind velocities: 1 m/s, 3 m/s, and 5 m/s. Regardless of whether they have isosceles triangle facades or not, all model buildings exhibit the minimum velocity on their front surfaces. This is due to the high pressure generated at the front of the structure, regardless of the presence of isosceles triangle facades. When setting the wind-inlet angle at 45° and the isosceles triangle facades at 45°, Figure 15 compares the velocity contour plots around the building model with and without isosceles triangle facades. Figure 16 demonstrates the comparison of velocity contour plots around the building model with and without isosceles triangle facades, when the wind-inlet angle is fixed at 90° and the facades are set at 45°. This result demonstrates that the wind direction directly influences the diversity of the velocity distribution around the building. Figures 17–19 illustrate a comparison of the pressure contour plots surrounding the building model. The comparison is conducted between the model without isosceles triangle facades and the model including isosceles triangle facades. The wind-inlet angle is maintained at 0°, while the isosceles triangle facades are at three distinct angles: 15°, 30°, and 45°. Its comparison was carried out at various wind velocities: 1 m/s, 3 m/s, and 5 m/s. Figure 20 exhibits the comparison of pressure contour plots around the building model with and without isosceles triangle facades, where the wind-inlet angle is kept at 45° and the facades are also set at 45°. Figure 21 shows a comparison of pressure contour plots surrounding the building model, both with and without isosceles triangle facades. The wind-inlet angle remains constant at 90° and the facades are at a 45°

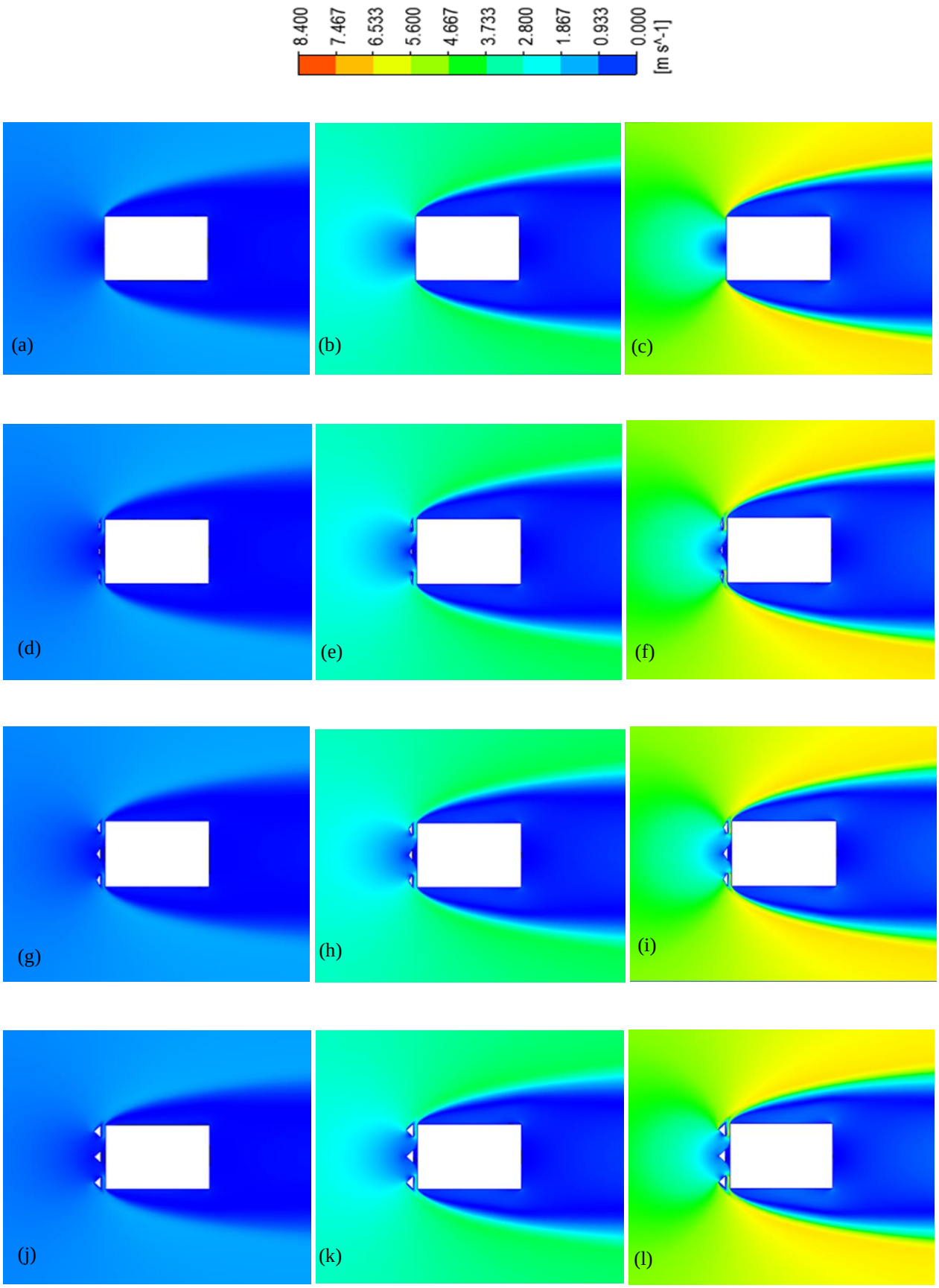

Fig. 12 collation of velocity distribution contour plots between building with and without facades for β = 0°, (a) no facades at U_∞= 1 m/s, (b) no facades at U_∞= 3 m/s, (c) no facades at U_∞= 5 m/s, (d) α = 15° at U_∞= 1 m/s, (e) α = 15° at U_∞= 3 m/s, (f) α = 15° at U_∞= 5 m/s, (g) α = 30° at U_∞= 1 m/s, (h) α = 30° at U_∞= 3 m/s, (i) f α = 30° at U_∞= 5 m/s, , (j) α = 45° at U_∞= 1 m/s, (k) α = 45° at U_∞= 3 m/s, (l) α = 45° at U_∞= 5 m/s

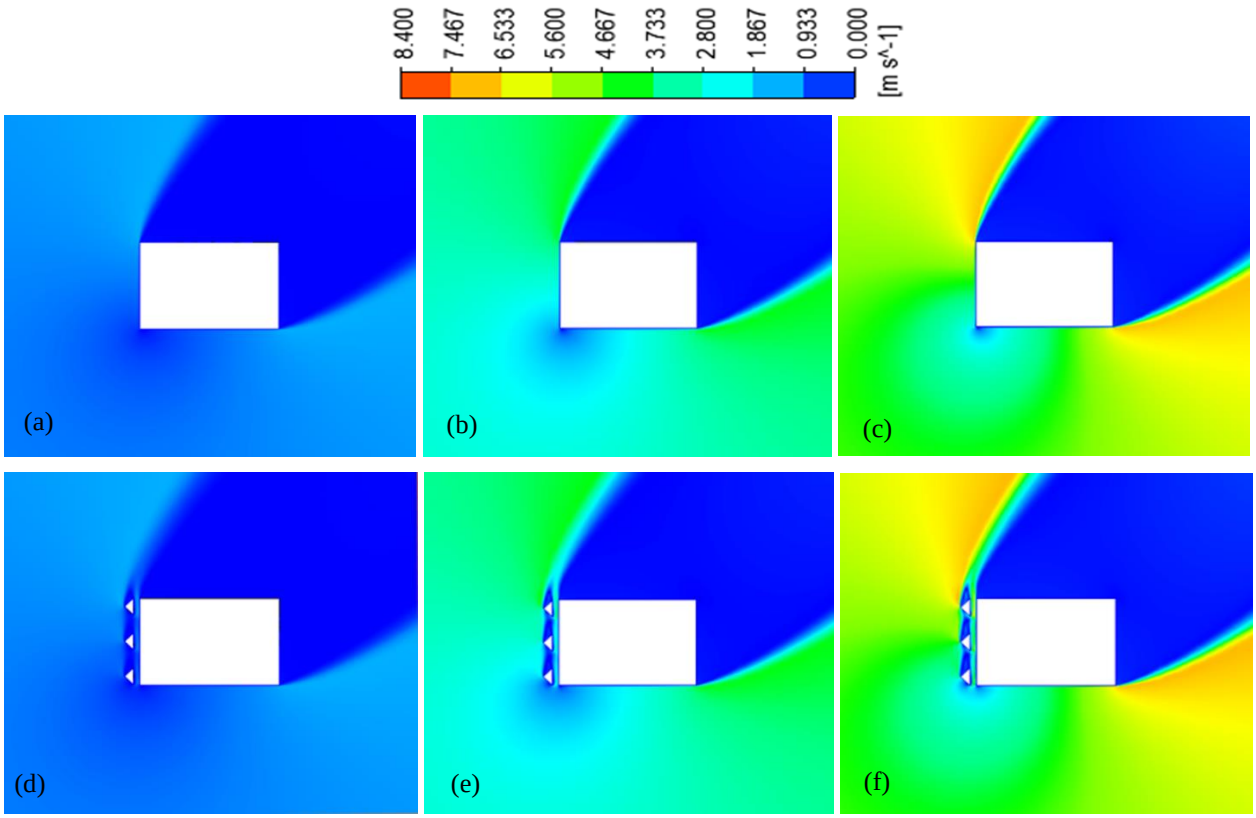

Fig. 13 collation of velocity distribution contour plots of building with and without facades for β = 45°, (a) no facades at U_∞= 1 m/s, (b) no facades at U_∞= 3 m/s, (c) no facades at U_∞= 5 m/s, (d) α = 45° at U_∞= 1 m/s, (e) α = 45° at U_∞= 3 m/s, (f) α = 45° at U_∞= 5 m/s

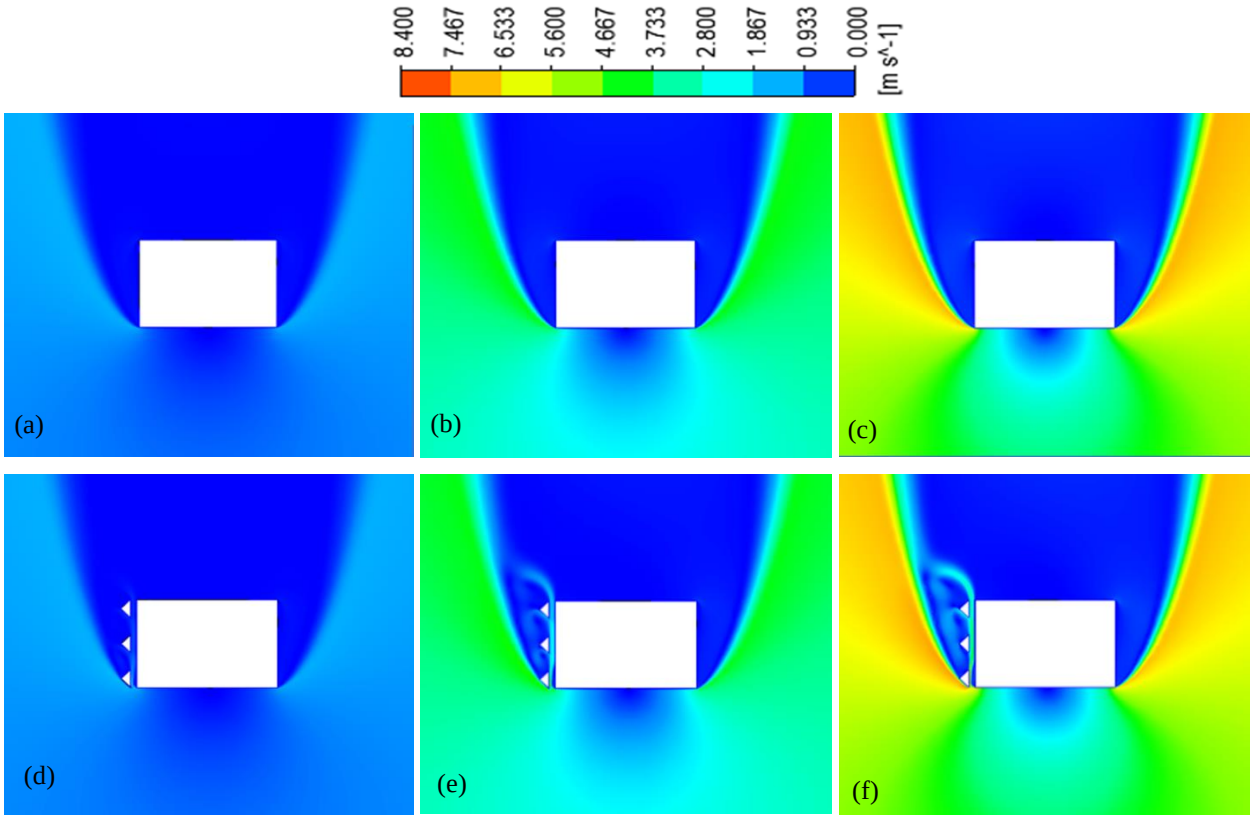

Fig. 14 collation of velocity distribution contour plots of building with and without facades for β = 90°, (a) no facades at U_∞= 1 m/s, (b) no facades at U_∞= 3 m/s, (c) no facades at U_∞= 5 m/s, (d) α = 45° at U_∞= 1 m/s, (e) α = 45° at U_∞= 3 m/s, (f) α = 45° at U_∞= 5 m/s

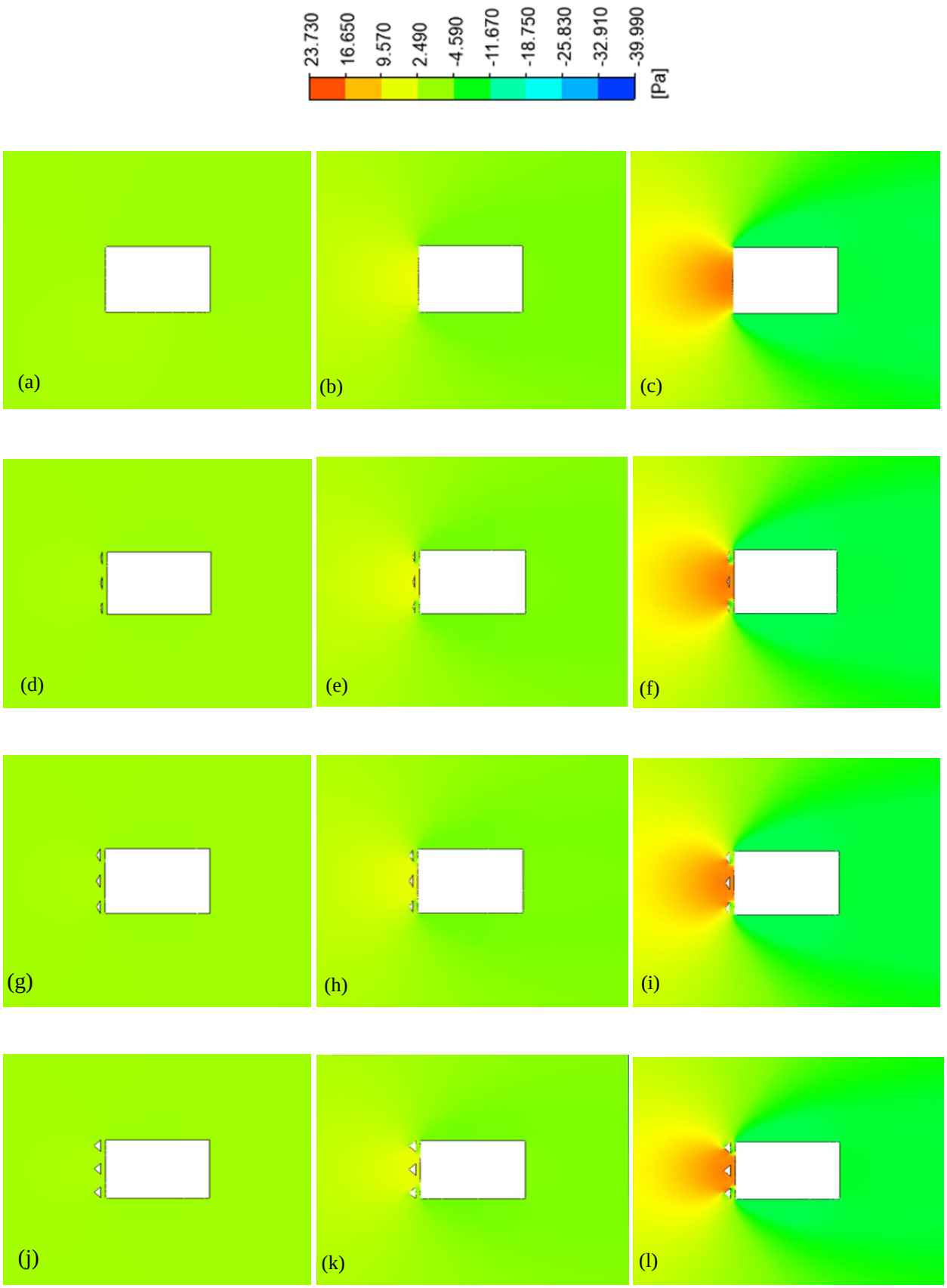

Fig. 15 collation of pressure distribution contour plots between building with and without facades for β = 0°, (a) no facades at U_∞= 1 m/s, (b) no facades at U_∞= 3 m/s, (c) no facades at U_∞= 5 m/s, (d) α = 15° at U_∞= 1 m/s, (e) α = 15° at U_∞= 3 m/s, (f) α = 15° at U_∞= 5 m/s, (g) α = 30° at U_∞= 1 m/s, (h) α = 30° at U_∞= 3 m/s, (i) α = 30° at U_∞= 5 m/s, , (j) α = 45° at U_∞= 1 m/s, (k) α = 45° at U_∞= 3 m/s, (l) α = 45° at U_∞= 5 m/s

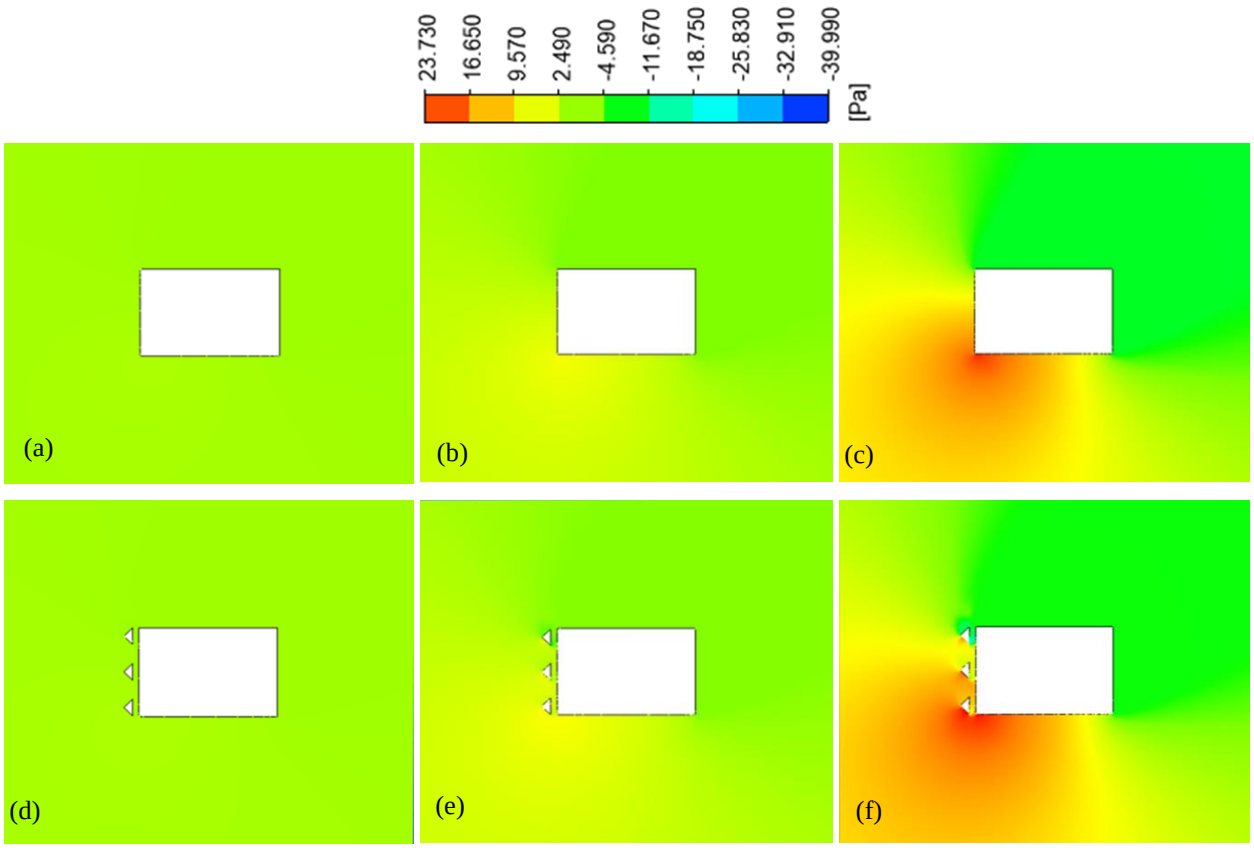

Fig. 16 collation of pressure distribution contour plots of building with and without facades for β = 45°, (a) no facades at U_∞= 1 m/s, (b) no facades at U_∞= 3 m/s, (c) no facades at U_∞= 5 m/s, (d) α = 45° at U_∞= 1 m/s, (e) α = 45° at U_∞= 3 m/s, (f) α = 45° at U_∞= 5 m/s

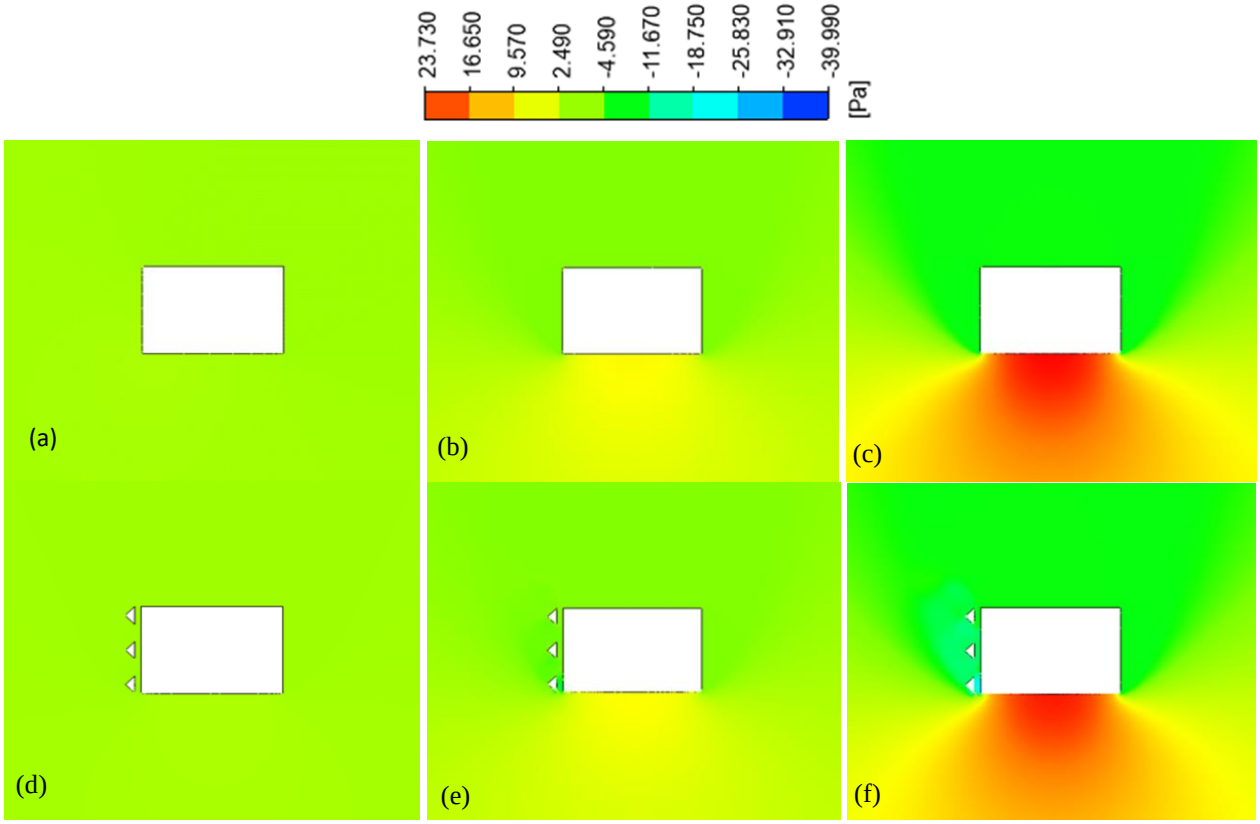

Fig. 17 collation of pessure distribution contour plots of building with and without facades for β = 90°, (a) no facades at U_∞= 1 m/s, (b) no facades at U_∞= 3 m/s, (c) no facades at U_∞= 5 m/s, (d) α = 45° at U_∞= 1 m/s, (e) α = 45° at U_∞= 3 m/s, (f) α = 45° at U_∞= 5 m/s

angle. All model buildings exhibit the maximum pressure on their front surfaces because this surface experiences airflow first. The maximum pressure occurs on the front surface of the building with a wind-inlet angle of 90° because the surface experiences a large amount of wind.

4. CONCLUSION

It is critical to use facades to improve energy savings, building design, local environmental conditions, and flow behaviors of buildings. The biggest goal of this study is to determine the optimal location for facades in relation to variations in wind load at U_∞ values of 1 m/s, 2 m/s, 3 m/s, 4 m/s, and 5 m/s. Sixty-five numerical simulations were carried out of the building with and without isosceles triangle facades using CFD models to enhance our understanding of the flow patterns around the building and its facades The results of drag forces on the building with and without isosceles triangle facades at three different angles (15°, 30°, and 45°) were considered when wind-inlet angles were set at 0°, 45°, and 90° and the distances between the front surface of the building and the facades were 0.01 m and 0.02 m. The results show that the drag forces of the building, both with and without isosceles triangle facades, are dependent on factors such as wind velocity, the angles of the isosceles triangle facades, the distances between the building's front surface and the facades, and the angle of the wind inlet. When wind velocity rises, the drag force acting on the building and its facades increases. As the angles of the isosceles triangle facade transition from 15° to 45°, the pressure forces generated on wall surfaces get smaller. The building with isosceles triangle facades at angles of 15° experiences greater total drag forces than the building with isosceles triangle facades at angles of 30° and 45°, regardless of wind velocity. When the distance between the front surface and the facades is 0.02 m, the building with isosceles triangle facades exhibits more total drag forces compared to when it is 0.01 m. The models' investigation reveals that the angle of the isosceles triangle facades significantly affects the drag force outcomes, compared to the distance between the building's front surface and the facades. The drag forces on a building with isosceles triangle facades at 45° angles, when facing a 90° wind direction, are higher than those in wind directions of 0° and 45°. The comparison of the numerical simulations points out that the wind-inlet angle, particularly at 90°, significantly influences the drag forces findings. The maximum drag forces on the building are obtained from the inlet airflow at an angle of 90° with the wind-inlet. A future study could consider all of a building enclosed by smart triangular facade systems and triangular facades capable of adjusting their angles to minimize drag forces on structures using CFD techniques. This data can provide important details for the design and placement of building facades to optimize their efficiency in reducing drag forces and creating more comfortable living environments for inhabitants.

CONFLICT OF INTEREST

The author declares that he has no conflicts of interest.

AUTHORS CONTRIBUTION

M. Tabatabaei Malazi and **K. Fakih**: Conceptualization, **M. Tabatabaei Malazi** and **K. Fakih**: methodology, **M. Tabatabaei Malazi** and **K. Fakih**: software, **M. Tabatabaei Malazi**: validation, **M. Tabatabaei Malazi** and **K. Fakih**: investigation, **M. Tabatabaei Malazi** and **K. Fakih**: data curation, **M. Tabatabaei Malazi** and **K. Fakih**: writing—original draft preparation

REFERENCES

Amani-Beni, M., Tabatabaei Malazi, M., Dehghanian, K., & Dehghanifarsani, L. (2023). Investigating the effects of wind loading on three-dimensional tree models using numerical simulation with implications for urban design. *Scientific Reports, 13*, 7277. https://doi.org/10.1038/s41598-023-34575-1

Amani-Beni, M., Tabatabaei Malazi, M., Sahin, B., & Dalkılıc, A. S. (2024). Effects of facades positioned at different angles on building thermal performance and flow behaviors. *Frontiers of Architectural Research*. https://doi.org/10.1016/j.foar.2024.08.001

ANSYS Fluent Theory Guide; ANSYS, Inc.: Canonsburg, PA, USA, 2016; pp. 39–136.

Attia, S., Bilir, S., Safy, T., Struck, C., Loonen, R., & Goia, F. (2018). Current trends and future challenges in the performance assessment of adaptive façade systems. *Energy and Buildings, 179*, 165-182. https://doi.org/10.1016/j.enbuild.2018.09.017

Batchelor, G. K. (2000). *An introduction to fluid dynamics*. Cambridge, UK: Cambridge University Press.

Bianchi, S., Andriotis, C., Klein, T., & Overend, M. (2024). Multi-criteria design methods in façade engineering: State-of-the-art and future trends. *Building and Environment*. *250*, 111184. https://doi.org/10.1016/j.buildenv.2024.111184

Chaudhry, H. N., Calautit, J. K., & Hughes, B. R. (2015). Computational analysis to factor wind into the design of an architectural environment. *Modelling and Simulation in Engineering*, 234601. https://doi.org/10.1155/2015/234601

Chen, F. B., Liu, H. M., Chen, W., Shu, Z. R., Li, Y., Li, Q. S., & Han, Y. (2022). Characterizing wind pressure on CAARC standard tall building with various façade appurtenances: An experimental study. *Journal of Building Engineering, 59*, 105015. https://doi.org/10.1016/j.jobe.2022.105015

Fuliotto, R., Cambuli, F., Mandas, N., Bacchin, N., Manara, G., & Chen, Q. (2010). Experimental and numerical analysis of heat transfer and airflow on an interactive building façade. *Energy and Buildings, 42*, 23-28. https://doi.org/10.1016/j.enbuild.2009.07.003

Hosseini, S. M., Mohammadi, M., & Guerra-Santin, O. (2019). Interactive kinetic façade: Improving visual comfort based on dynamic daylight and occupant's

positions by 2D and 3D shape changes. *Building and Environment, 165*, 106396. https://doi.org/10.1016/j.buildenv.2019.106396

Hou, F., & Sarkar, P. P. (2018). A time-domain method for predicting wind-induced buffeting response of tall buildings. *Journal of Wind Engineering and Industrial Aerodynamics, 182*, 61-71. https://doi.org/10.1016/j.jweia.2018.09.017

Hou, F., Sarkar, P. P., & Alipour, A. (2023). A novel mechanism - smart morphing façade system - to mitigate wind-induced vibration of tall buildings. *Engineering Structures, 275*, Part A, 115152. https://doi.org/10.1016/j.engstruct.2022.115152

Jafari, M., & Alipour, A. (2021). Aerodynamic shape optimization of rectangular and elliptical double-skin façades to mitigate wind-induced effects on tall buildings. *Journal of Wind Engineering and Industrial Aerodynamics, 213*, 104586. https://doi.org/10.1016/j.jweia.2021.104586

Lops, C., Germano, N., Matera, S., D'Alessandro, V., & Montelpare, S. (2021). CFD Modelling of naturally ventilated double skin façades: Comparisons among 2D and 3D models. *TECNICA ITALIANA-Italian Journal of Engineering Science, 65*, 330–336. https://doi.org/10.2495/TE050421

Mallick, M., Mohanta, A., Kumar, A., & Raj, V. (2018). Modelling of wind pressure coefficients on C-shaped building models. *Modelling and Simulation in Engineering, 2018*, 6524945. https://doi.org/10.1155/2018/6524945

Olcay, A. B., & Tabatabaei Malazi, M. (2016). The effects of a longfin inshore squid's fins on propulsive efficiency during underwater swimming. *Ocean Engineering, 128*, 173–182. https://doi.org/10.1016/j.oceaneng.2016.09.011

Pasut, W., & De Carli, M. (2012). Evaluation of various CFD modelling strategies in predicting airflow and temperature in a naturally ventilated double skin façade. *Applied Thermal Engineering, 37*, 267-274. https://doi.org/10.1016/j.applthermaleng.2011.11.024

Pomaranzi, G., Daniotti, N., Schito, P., Rosa, L., & Zasso, A. (2020). Experimental assessment of the effects of a porous double skin façade system on cladding loads. *Journal of Wind Engineering and Industrial Aerodynamics, 196*, 104019. https://doi.org/10.1016/j.jweia.2019.104019

Škvorc, P., & Kozmar, H. (2023). The effect of wind characteristics on tall buildings with porous double-skin façades. *Journal of Building Engineering, 69*, 106135. https://doi.org/10.1016/j.jobe.2023.106135

Soudian, S., & Berardi, U. (2021). Development of a performance-based design framework for multifunctional climate-responsive façades. *Energy and Buildings, 231*, 110589. https://doi.org/10.1016/j.enbuild.2020.110589

Tabatabaei Malazi, M., Eren, E. T., Luo, J., Mi, S., & Temir, G. (2020). Three-dimensional fluid–structure interaction case study on elastic beam. *Journal of Marine Science and Engineering, 8*(9), 714. https://doi.org/10.3390/jmse8090714

Yi, H., & Kim, Y. (2021). Prototyping of 4D-printed self-shaping building skin in architecture: Design, fabrication, and investigation of a two-way shape memory composite (TWSMC) façade panel. *Journal of Building Engineering, 43*, 103076. https://doi.org/10.1016/j.jobe.2021.103076

Yuan, K., Hui, Y., & Chen, Z. (2018). Effects of facade appurtenances on the local pressure of high-rise building. *Journal of Wind Engineering and Industrial Aerodynamics, 178*, 26-37. https://doi.org/10.1016/j.jweia.2018.05.003

Zhao, X., Wei, A., Zou, S., Dong, Q., Qi, J., Song, Y., & Shi, L. (2024). Controlling naturally ventilated double-skin façade to reduce energy consumption in buildings. *Renewable and Sustainable Energy Reviews. 202*, 114649. https://doi.org/10.1016/j.rser.2024.114649